PRE-PRINT version. Cite this article as:

H.M. Saif, R.M. Huertas, S. Pawlowski, J.G. Crespo, S. Velizarov, Development of highly selective composite polymeric membranes for Li^+/Mg^{2+} separation, *Journal of Membrane Science*, 620 (2021) 118891 https://doi.org/10.1016/j.memsci.2020.118891

Development of highly selective composite polymeric membranes for Li^+/Mg^{2+} separation

H.M. Saif[1], R.M. Huertas[1,2,*], S. Pawlowski[1, *], J.G. Crespo[1], S. Velizarov[1]

[1]LAQV-REQUIMTE, DQ, FCT, Universidade NOVA de Lisboa, 2829-516 Caparica, Portugal

[2]iBET, Instituto de Biologia Experimental e Tecnológica, Apartado 12, 2780-901 Oeiras, Portugal

*Corresponding authors: E-mail: rosa.huertas@ibet.pt (R.M. Huertas), s.pawlowski@fct.unl.pt (S. Pawlowski).

ABSTRACT

To meet the exponentially rising demand for lithium, it becomes indispensable to develop environmental friendly processes for its recovery from brines and/or seawater. In this work, novel composite lithium transport selective polymeric membranes were developed to separate lithium and magnesium ions. Hydrogen manganese oxide (HMO), polystyrene sulfonate sodium salt (PSS-Na) and lithium triflate ($LiCF_3SO_3$) were added into a synthesized sulfonated polyethersulfone (SPES) matrix to prepare composite membranes. The developed membranes showed a high mechanical stability and a homogeneous distribution of HMO. The most promising membrane, containing 20 % (w/w) of HMO, showed almost 20 times higher Li^+ ionic conductivity (8.28×10^{-3} S/cm) compared to that of a reference standard commercial cation exchange membrane and an average ideal selectivity of 11.75 for Li^+/Mg^{2+}

pair. Moreover, the lithium ion transport performance and separation efficiency were investigated through diffusion dialysis experiments, under different operating conditions. A binary separation factor of 9.10 for Li^+/Mg^{2+} and Li^+ molar flux of 0.026 mol/(m^2.h) were achieved without applying an external potential difference. When an external potential difference of 0.2 V was applied, the binary separation factor of Li^+/Mg^{2+} pair decreased to 5.00, while the Li^+ molar flux increased almost 5 times. The obtained results provide the basis to design and develop composite lithium transport selective polymeric membranes and represent a promising step for future implementation of such membranes to recover lithium from brines and/or seawater.

KEYWORDS

Lithium recovery, Composite membranes, Lithium ion sieves (LIS), Sea mining, Diffusion dialysis

1. INTRODUCTION

Lithium finds application in a very wide spectrum of industries such as pharmaceutical, metallurgy, ceramic and glass [1–4], but it is its use in batteries, employed in the electronic devices and electric cars, that suddenly increased the market demand for lithium carbonate [5,6]. Lithium can be extracted from land reserves (by methods harsh for the environment) and/or from aqueous streams such as brines and seawater (by low-efficiency evaporation processes) [7–9].

Membrane technologies offer environmental friendly separation options, with a relatively low energy costs and negligible use of chemicals, compared to conventional processes [10]. Ion exchange membranes (IEM), with a tailored selectivity towards a specific ion, stand out as a possible solution to selectively separate lithium from other accompanying cations, such as sodium, potassium and magnesium, present in aqueous streams. Polymeric ion exchange membranes, for instance sulfonated polyethersulfone membranes, poly(ethylene-co-vinyl alcohol) membranes and poly(ethylene

terephthalate) membranes have been reported for Li^+ recovery from brines. However, the exhibited Li^+/Mg^{2+} separation factor of these membranes was below 1.5 [11,12]. Guo et al. [13] developed a metal-organic framework (MOF) on a threaded sulfonated polymer achieving a very high Li^+/Mg^{2+} binary separation factor of 1815. However, the very brittle nature of the MOF film limits its use on a large scale. Hoshino [14] reported the use of ionic superconductor type crystals as a ceramic membrane in a dialysis process for lithium recovery from seawater but, due to a low membrane conductivity, the lithium recovery rate was very slow. Moreover, the mechanical stability of these membranes was limited.

Alternatively, a class of materials called lithium ion sieves (LIS), which are inorganic adsorbents such as $Li_{1.6}Mn_{1.6}O_4$, $Li_{1.33}Mn_{1.67}O_4$ (LMO compounds) and λ-MnO_2, demonstrated a high Li^+ selectivity and an adsorption capacity of up to 40 mg/g [3]. This was attributed to the presence of special lithium transferring channels in the spinel type manganese dioxide frameworks, which act as a lithium ion sieve, because of the existence of cavities in the LMO crystal structure, which size only matches with Li^+ and excludes bigger cations like Na^+, K^+ and Ca^{2+} [2]. Although the crystallographic sizes of Mg^{2+} and Li^+ are similar, Mg^{2+} does not enter into the LMO cavities due to its much higher hydration energy [15,16]. To the best of our knowledge, the incorporation of LIS into cation exchange membranes (CEMs) has been so far reported only by Zhang et al. [16] achieving a Li^+/Mg^{2+} separation factor of 3.1 when hydrogen manganese oxide (HMO) was dispersed into a sulfonated polyether ether ketone.

Herein, we report a method to produce chemically, mechanically and thermally stable composite lithium transport selective polymeric membranes by dispersing hydrogen manganese oxide (HMO) into sulfonated polyethersulfone, with the addition of a sodium salt of polystyrene sulfonate (PSS-Na) and lithium salt ($LiCF_3SO_3$). The transport of lithium through the developed membranes was assessed via a comparison of current-voltage curves and results of diffusion dialysis experiments, performed with and without applying an external potential difference.

2. MATERIALS AND METHODS

2.1. Materials

Lithium carbonate (Li_2CO_3, Sigma-Aldrich, 99.9 %) and manganese carbonate ($MnCO_3$, Sigma-Aldrich, 99.5 %) were used to prepare the LMO adsorbent. Commercial polyethersulfone (PES) (Ultrason® E6020P), purchased from BASF, was chosen to prepare polymer matrix. Chlorosulfonic acid (CSA) ($ClSO_3H$, Sigma-Aldrich, 97 %) and sulfuric acid (H_2SO_4, 97 %) were used to promote the sulfonation of the PES backbone. Dimethylformamide (DMF, Sigma-Aldrich, 99.5 %) was used as a solvent. Lithium triflate ($LiCF_3SO_3$, Alfa Aesar, 99.5 %) was used as a bulky anion plasticizer to induce polymer flexibility. Hydrochloric acid (HCl, Sigma-Aldrich, 37 %) was used to protonate the lithium selective adsorbent. Lithium chloride (LiCl, Alfa Aesar, 99.9 %) and magnesium chloride ($MgCl_2$, Sigma-Aldrich, 99 %) were used to prepare the working solutions. Sodium hydroxide (0.01 M NaOH, Sigma-Aldrich, 97 %) standard solution and phenolphthalein (Sigma-Aldrich, 0.5 w% in ethanol : water (1:1)) were used in titration experiments. All reagents were used as received.

2.2. Preparation of composite membranes

Composite membranes were prepared in three steps (Figure 1). In steps 1 and 2 HMO and SPES were prepared, respectively, while in step 3 HMO, PSS-Na and $LiCF_3SO_3$ were incorporated into SPES and the formed membranes were labelled as Composite-X% where X is the weight percentage of HMO to SPES (X= 0, 5, 10, 15, 20, 25 %).

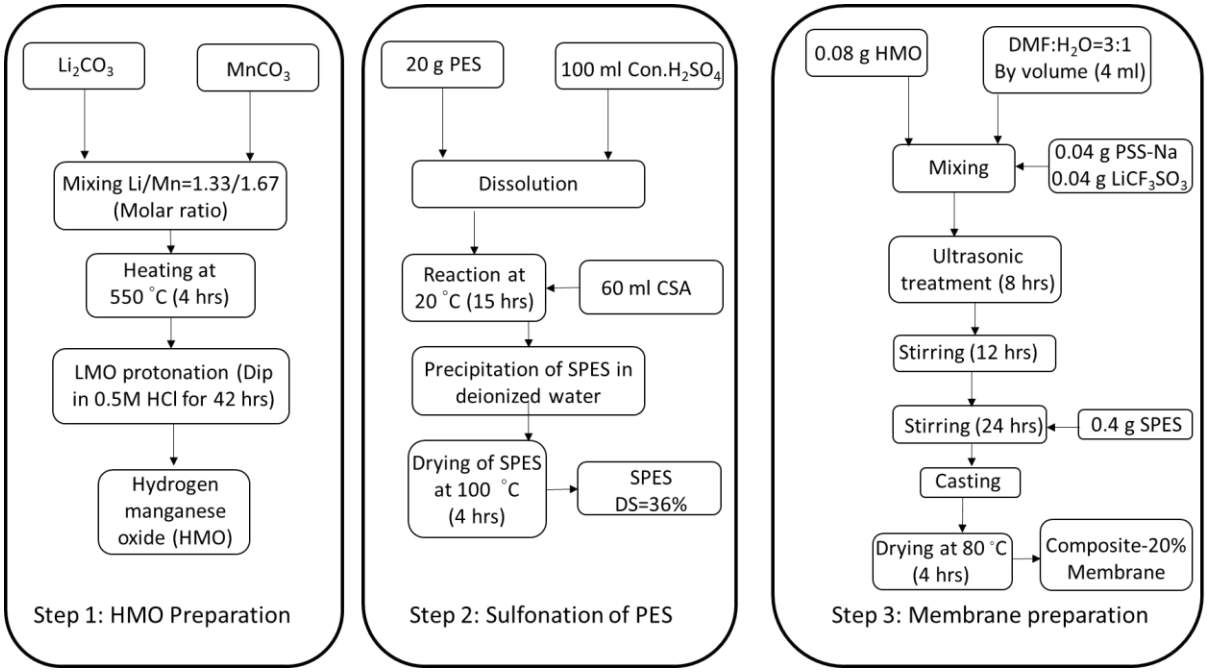

Figure 1. Steps followed in the preparation of composite-20% membrane.

2.2.1. Synthesis of HMO

The solid-state fusion method was used to prepare the lithium manganese oxide LMO ($Li_{1.33}Mn_{1.67}O_4$) powder. Li_2CO_3 and $MnCO_3$ with a molar ratio of Li/Mn = 1.33/1.67 were well mixed in a mortar and the prepared reaction mixture was placed in a ceramic boat and heated in an oven for 4 hours at 550 °C under air atmosphere [17,18]. Afterward, Li^+ was extracted from the LMO adsorbent to convert into its protonated form by dissolving 5 g of LMO in HCl solution (0.5 M, 500 mL) stirred for 42 hours at room temperature. The resultant mixture was filtered through a 0.4 micron ceramic filter and washed several times with deionized water until achieving a neutral pH. The filter cake was air-dried at 70 °C for 24 hours [19].

2.2.2. Sulfonation of PES

Polyethersulfone (PES) was selected as a polymer matrix because of its excellent thermal, mechanical and chemical properties (abundant sulfonate groups and high chemical resistance) and relatively low cost [20]. Chlorosulfonic acid (CSA) was used as a sulfonating agent since it is less expensive and allows for a uniform electrophilic substitution, so there is no need for additional post-treatment, in contrast to the other sulfonating reagents like SO_3 and Oleum [21]. 20 g of PES was dissolved under stirring in 100 ml of concentrated sulfuric acid (97 %) at room temperature to form a homogeneous solution. Subsequently, 60 ml of chlorosulfonic acid (CSA) was added gradually dropwise into the reaction mixture with continuous vigorous stirring at a constant temperature of 20 °C using an ice bath. The sulfonation reaction was time-dependent and an optimal 36 % of sulfonation degree (DS) was achieved after 15 hours, as analysed by ^{1}H-NMR (section 2.3.2.1.). Final SPES polymer was obtained by gradual precipitation of the reaction mixture into ice-cold deionized water. The precipitates were recovered by filtration through a 50 mesh screen and washed with de-ionized water until the pH value 7 was achieved. The final product was dried in an oven at 100 °C for 4 hours.

2.2.3. Membranes preparation

The degree of sulfonation (DS) of PES is limited to 40 %, above this value, it starts to dissolve in water. Thus, the PSS-Na was introduced to increase the number of sulfonating groups in the membrane structure. Since the increase of DS also leads to an increase of crystallinity of the polymer matrix and, as a result, the membrane may become brittle, lithium salt ($LiCF_3SO_3$) was incorporated to increase the flexibility of the final structure of the membrane [22]. Previously prepared SPES, with DS=36 %, and HMO were used for membrane fabrication. Both, PSS-Na and $LiCF_3SO_3$, have poor solubility in pure DMF, thus, to prepare a homogeneous solution for membrane casting, deionized water with DMF in a volume ratio 1:3 was used as a solvent to prepare the films. A pre-defined quantity of HMO (X), 0.04 g PSS-Na and 0.04 g $LiCF_3SO_3$ were dispersed in 4 ml of solvent. The quantities of PSS-Na and

$LiCF_3SO_3$ were optimised to grant good mechanical stability of the membranes. The obtained mixtures were subjected to ultrasonic treatment for 8 hours to achieve uniform dispersion of the components. Afterward, the solutions were stirred vigorously for 12 hours, 0.4 g of SPES was added and again the mixture was stirred for another 24 hours to achieve a homogeneous solution. The formed solution was casted on a glass petri dish and dried at 45 °C for the first 12 hours, at 60 °C for the next 12 hours and finally at 80 °C for the last 6 hours. The synthesized membranes were immersed for 24 hours in a 0.1 M HCl solution to leach out the remaining Li^+ and Na^+ ions. The amount of both ions in HCl solution was the same after 24 and 48 hours, thus there was no additional leaching of lithium and sodium after 24 hours. Finally, the membranes were thoroughly washed with deionized water several times and dried in an oven at 80 °C for 4 hours. The thickness of the prepared membranes was 100 µm ± 5 µm.

2.3. Membranes characterization

Composite membranes were characterized to analyse their ion transport performance, ideal selectivity, binary separation factor, morphology, chemical composition (chemical stability), contact angle (hydrophilicity), water uptake, and thermal and mechanical properties. The membranes were tested twice, as pristine and after being used for 10 hours in diffusion experiments.

2.3.1. Evaluation of lithium transport

The performance of the prepared composite membranes and a standard Selemion™ CEM membrane acquired from AGC Engineering (Japan) was compared in terms of their ideal selectivity and binary separation factor. Experiments were performed using a cylindrical electrochemical cell with 2 compartments of 186 ml capacity each (Figure 2). The active membrane area in the cell was 11.34 cm^2. Copper rods were used as electrodes. Ionic composition of the feed and the receiver was analysed

by inductively coupled plasma atomic emission spectroscopy (ICP-AES). Samples (2 ml each) were taken after 5 hours from the two compartments of the electrochemical cell.

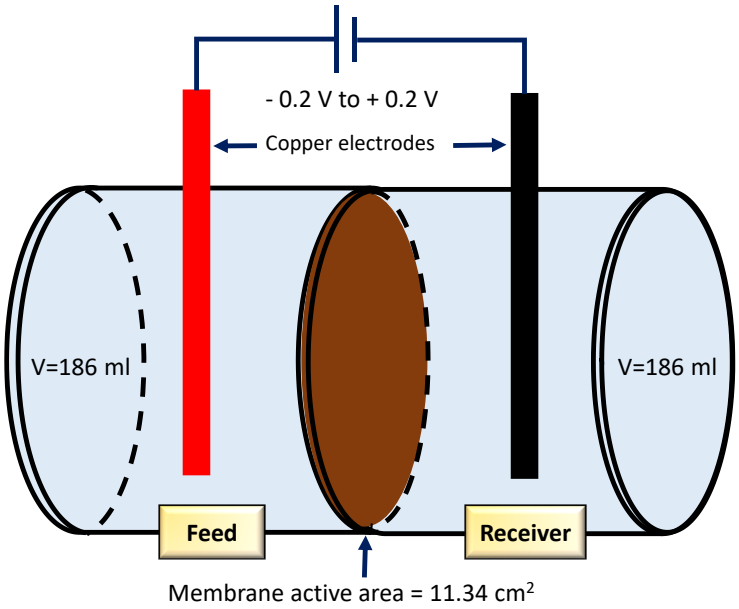

Figure 2. A schematic configuration of the electrodialysis cell.

2.3.1.1. Ideal selectivity

The ideal selectivity values for Li^+/Mg^{2+} were evaluated via current-voltage curves obtained through linear sweep voltammetry (LSV), by Vertex 5A potentiostat (Ivium Technologies). A scan rate of 200 mV/s, at a step of 1 mV for the potential difference range between - 0.2 V and + 0.2 V were used as LSV operating conditions. In these experiments, the feed and the receiver side of the electrochemical cell contained the same salt solution (0.1 M LiCl or 0.1 M $MgCl_2$). The membranes under study were equilibrated for one hour in the respective salt solution before measuring the current-voltage (I-V) curves. The slope of the linear part of the I-V curve gives the conductance value of the membrane immersed in a given salt solution. The ratio of slops of I-V curves obtained for different salt solutions gives the ideal selectivity of counter-ions (in the present case Li^+/Mg^{2+}) pair.

2.3.1.2. Binary separation factor

The binary separation factor between lithium and magnesium was defined as a ratio of their degrees of recovery in the receiver:

$$Binary\ separation\ factor = \frac{[Li^+]\ (receiver, t = t) \Big/ [Li^+]\ (feed, t = 0)}{[Mg^{2+}]\ (receiver, t = t) \Big/ [Mg^{2+}]\ (feed, t = 0)} \qquad (\text{eq. } 1)$$

The binary separation factor was examined by using equimolar solutions of 0.25 M of LiCl and 0.25 M $MgCl_2$ in the feed compartment and deionized water in the receiver. These experiments were conducted under two different diffusion dialysis operating conditions: without applying potential difference and with an applied potential difference of + 0.2 Volts across the investigated membrane for 5 hours.

2.3.2. Chemical properties analysis

2.3.2.1. Degree of sulfonation (DS) and ion exchange capacity (IEC)

The degree of sulfonation (DS) was calculated and compared through titration and a nuclear magnetic resonance of proton (^{1}H-NMR) technique.

The first approach was to use the traditional titration method as follows: 0.5 g of polymer was dissolved in 10 ml of N, N-dimethylformamide (DMF) for complete liberation of protons (H^+). The released H^+ was titrated against 0.01 M NaOH standard solution using phenolphthalein as an indicator [21]. The ion exchange capacity was evaluated by using the degree of sulfonation value (eq.3) [23,24]. The following equations were applied:

$$DS\ (\%) = \left(\frac{0.232\ M_{NaOH} \times V_{NaOH}}{[W - (0.08\ M_{NaOH} \times V_{NaOH})]}\right) \times 100 \qquad (\text{eq. } 2)$$

$$IEC = \frac{1000 \times DS}{[(232 + 81) \times DS]} \qquad (\text{eq. } 3)$$

where M_{NaOH} is the molarity (mol/l) of standard NaOH solution, V_{NaOH} is the volume of NaOH (ml) , W is the dry sample weight (g), 232 is the molecular weight of PES repeating unit and 81 is the molecular weight of $–SO_3H$ [23].

In the second approach, ^{1}H-NMR spectra were recorded in 32 scans by applying π/2 (^{1}H) pulses and a delay time of 10 s on an Avance III 500 spectrometer (Bruker, Germany). Samples were prepared by dissolving 10 mg of dried PES in 0.6 ml DMSO-d6. The operating frequency of 500.13 MHz was used to obtain ^{1}H-spectra. 5 mm outer diameter NMR tubes were used for all the measurements at 30 ˚C. ^{1}H-NMR spectrum of modified polymer SPES was logged only in aromatic protons region because this is the location where sulfonating agent attacks easily and replace the aromatic proton of the Ortho-position with a sulfonic acid group with respect to the ether oxygen atom in the main chain [25].

The DS value was calculated by using the following formula [26]:

$$DS\ ({}^1_0H) = \frac{2I\ (H_{3'})}{I\ (H_{9+9^*})} \qquad (\text{eq. } 4)$$

2.3.3. Physical properties analysis

2.3.3.1. Water content

A piece of a dry membrane with dimension 1×1 cm^2 was immersed in deionized water for 24 hours and weighed after removing excessive water on both surfaces with filter paper. The wet membrane was placed in the vacuum oven at 60 °C for 24 hours and weighed again. The percentage of water content (WC) was determined as [24]:

$$WC\ (\%) = \frac{W_{wet} - W_{dry}}{W_{dry}} \times 100 \qquad (\text{eq. } 5)$$

2.3.3.2. Membrane hydrophilicity

The hydrophilicity of the synthesized membranes was examined by contact angle measurements using a goniometer (Dyne technology, UK) coupled with a KSV CAM2008 equipment. Before analysis, each membrane sample with a dimension 2×2 cm^2 was washed with deionized water and dried overnight, at room temperature, in a desiccator. A sessile drop of deionized water (10-12 µL) was placed on the membrane surface. Each measurement was attained with 20 frames with a frame interval of 100 ms. For each membrane, the average value of the contact angle was calculated from the measurements taken at three different points.

2.3.4. Structural and morphological properties

2.3.4.1. Fourier transform infrared spectroscopy (FT-IR)

Fourier Transform Infrared Spectra (FT-IR) using attenuated total reflectance (ATR) mode was employed to determine the chemical structure of the prepared composite membranes and the lithium selective adsorbent. The spectra were recorded at both sides of the membranes when pristine and after use (10 hours in diffusion dialysis experiments), to observe any structural modification which may have occurred during the experiments. The equipment employed was a Bruker Spectrometer IFS 66/S FT-IR instrument (USA) equipped by H-ATR with ZnSe crystal. Before analysing, the membrane samples were dried overnight in a desiccator at room temperature. The samples were taken from random positions of the membrane to check the homogeneity of the structure. The normalized spectra were recorded in the range of wave numbers from 4000 to 500 cm^{-1} during 20 scans with a 2 cm^{-1} resolution.

2.3.4.2. Crystallinity

The crystalline phases of the composite membrane were examined by X-ray diffraction patterns. These diffraction patterns were documented on a MiniflexII diffractometer (Rigaku, Japan) using

monochromatic Cu Kα radiation (λ = 1.542 Å, 30 kV, 15 mA). The average distance between the polymer chains or spacing between the crystalline phases (d) associated with the maximum peaks, was calculated using the Bragg equation:

$$n\lambda = 2d \cdot Sin\theta_{max} \quad (\text{eq. } 6)$$

where λ = 1.542 Å and 'n' is an integer and represents the order of reflection [27].

2.3.4.3. Morphological characterization

To evaluate the morphology of the composite membranes before and after use, a quantitative analysis and elemental chemical analysis were carried out using a Carl Zeiss AURIGA Cross Beam FIB-SEM workstation. Samples were prepared by cryogenic fracture under liquid nitrogen and made electrically conductive using a Sputter Quorum with 15 nm thick Au/Pd film.

2.3.5. Thermal properties analysis

2.3.5.1. Thermogravimetric analysis (TGA)

A TGA Q-50 analyzer (TA Instruments, USA) was employed to determine the degradation temperature and inorganic content using a ramp of 10.0 ˚C/min, in the temperature range of 25 to 600 ˚C under a nitrogen atmosphere with a flow rate of 40.0 ml/min. The approximate sample weight was 5.0 mg placed into an aluminium sample pan. The inorganic content and thermal behaviour of the membranes were analysed from TGA curves.

2.3.5.2. Differential scanning calorimetry (DSC)

The glass transition temperature (T_g) of the modified polymer and the composite membranes was calculated from differential scanning calorimetry (DSC). The DSC analysis was performed on a TA DSC Q-200 equipment (TA Instruments, USA). The temperature range of 0–300 ˚C was set in the DSC analysis, based on the polymer degradation data obtained from previous TGA study. Prior to the

analysis, the samples were dried in a desiccator and the approximate weight of each sample was 8.0 mg. The analysis was carried out in a nitrogen atmosphere with a flow rate of 40.0 ml/min and a heating rate of 20 °C /min. The inflection point of the variation in the specific heat was taken as T_g.

2.3.6. Mechanical properties analysis

2.3.6.1. Vickers Micro-hardness (MHV)

The mechanical properties of the composite membranes were analysed by testing the micro-hardness of the samples using ZHVμ Micro Vickers Hardness Tester. Six measurements were taken at room temperature over a smooth and clean surface of each sample and the mean value was reported. A square-based pyramid diamond was used as an indenter with 0.05 kg_f applied load on the material surface for 15 seconds. Vickers micro-hardness value (in kg_f/mm^2) was calculated by using the following formula:

$$MH = \frac{2Sin68^{\circ} \times F}{d^2} \qquad (\text{eq. } 7)$$

where F (kg_f) is the applied load and d (mm) is the diagonal length of the indentation area on the tested sample [28]. The tensile strength was calculated by using the following correlation [29,30]:

$$MH = 2.33 \times \sigma_y \qquad (\text{eq. } 8)$$

where MH is the hardness in MPa and σ_y is the tensile strength in MPa units.

3. RESULTS AND DISCUSSION

3.1. Lithium selectivity

3.1.1. Ideal selectivity

The I-V curves of all the synthesized membranes and of the commercial Selemion CEM are presented in Figure 3a and 3b, while the corresponding ideal selectivities, calculated from ion conductivity data (Figure 3c), are shown in Figure 3d.

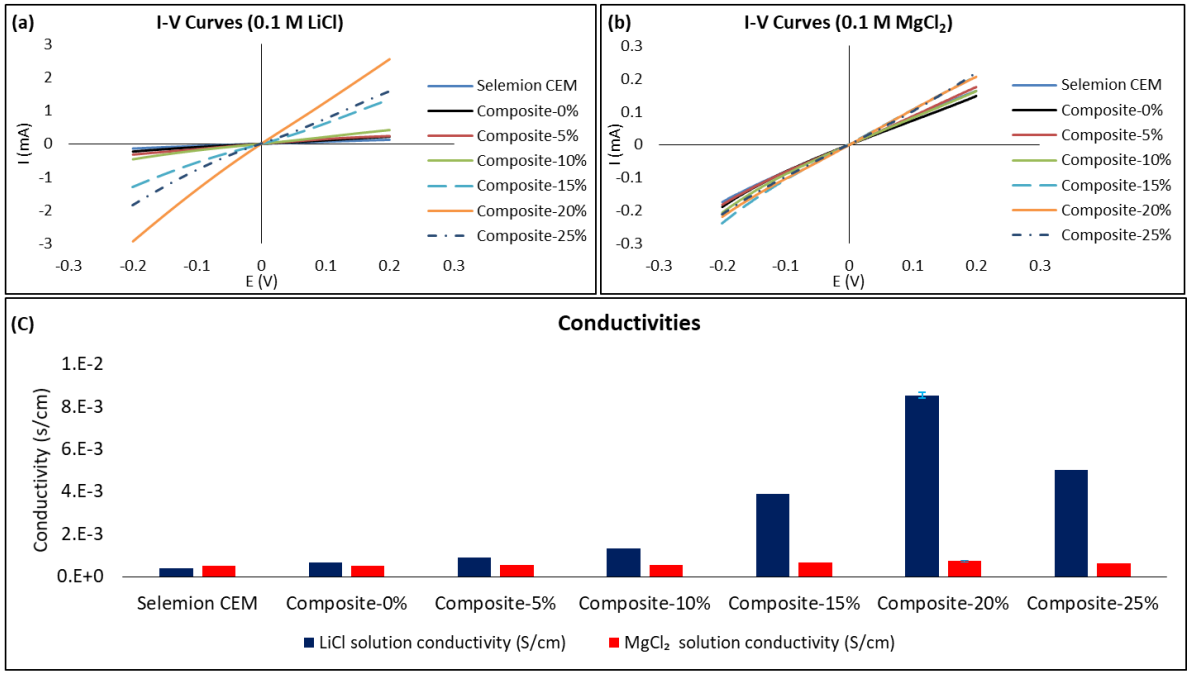

(d)

Membranes	Selemion™	Comp-0%	Comp-5%	Comp-10%	Comp-15%	Comp-20%	Comp-25%
Li^+/Mg^{2+}	0.78	1.34	1.67	2.39	5.77	11.75 ± 0.55	7.89

Figure 3. (a) I-V curves 0.1M LiCl (b) I-V curves 0.1M $MgCl_2$ (c) LiCl and $MgCl_2$ solutions conductivities (d) Li^+ ion ideal selectivity.

In the commercial Selemion™ cation exchange membrane, Mg^{2+} ions migrate faster than Li^+ ions (Figure 3c) because they interact electrostatically more strongly with the membrane's negative fixed groups, due to their divalent nature, comparing to the monovalent ions. In the prepared composite membranes, the incorporation of HMO changed this, as for example, merging just 5% w/w of HMO into the composite membrane increased twice the Li^+ ion conductivity of that membrane, while the Mg^{2+} conductivity remained almost the same. Likewise, the Li^+ ion conductivity continuously increased with the increase in HMO content from 5% w/w to 20% w/w and a Li^+/Mg^{2+} ideal selectivity close to 12 was achieved (Figure 3d), which is a value almost 4 times higher than previously achieved [16]. The sharp increase of Li^+ conductivity with increasing HMO content can be explained by the HMO structure

which only allows the free insertion of Li^+ through its 8a-16d-8a interspaces and the synergistic effect of sulfonating groups of the polymer, which have different binding affinity with different cations such as Li^+=1.0, Na^+=1.98, K^+=2.9 and Mg^{2+}=3.18 (all these values are normalized to Li^+) [12,16]. However, further increment in HMO content to 25% w/w led to a reduction of Li^+ conductivity, which is not unexpected, as the inorganic filler can block ionic channels in the polymer matrix hindering the diffusion of molecules or ions through the membrane [31].

Since the Composite-20% membrane showed the highest ideal selectivity for lithium, therefore, the results for that membrane are shown in the following sections.

3.1.2. Binary separation factor and cationic flux

Figures 4a and 4b show the data related to lithium and magnesium molar ionic fluxes and their binary separation factor by Composite-20% membrane.

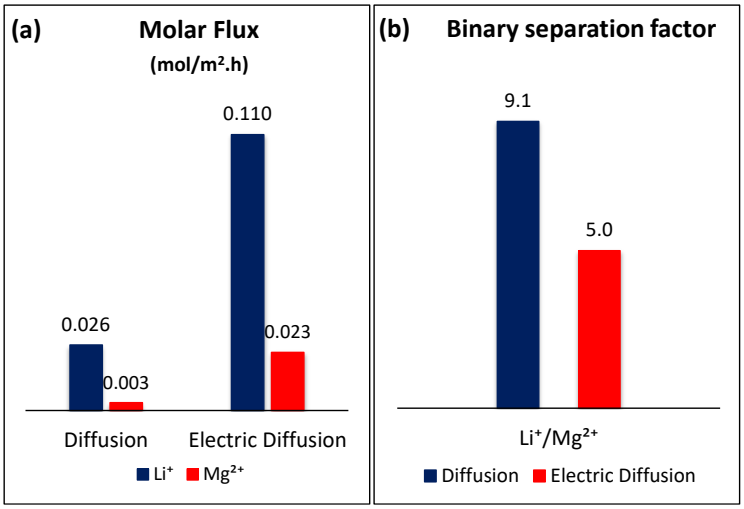

Figure 4. (a) Li^+ and Mg^{2+} ion fluxes in diffusion and electric diffusion experiments, (b) Binary separation factor of Li^+/Mg^{2+} pair by composite-20% membrane.

For diffusion dialysis, the binary separation factor was 9.1 and the lithium molar flux was 0.026 mol/(m^2.h). When an external potential difference of 0.2 V was applied, the binary separation factor decreased to 5, but the Li^+ molar flux increased almost 5 times (0.11 mol/(m^2.h)). In both cases, a lower Mg^{2+} flux could be due to its bigger hydrated size, lower diffusion coefficient and higher binding affinity to sulfonic groups compared to that of Li^+ [13]. When the external potential difference was applied, the external force and the selective nature of the membrane boosted the Li^+ flux but the flux of Mg^{2+} also increased significantly, possibly because Mg^{2+} is doubly charged so it experiences the double of the electric force (compared to Li^+), which could increase its transport by migration.

3.2. Membrane characterization

3.2.1. Ion exchange capacity and degree of sulfonation

The degree of sulfonation (DS) of the polymer matrix (SPES) used to prepare the composite membranes was measured by two independent methods: titration and ^{1}H-NMR (Figure 5).

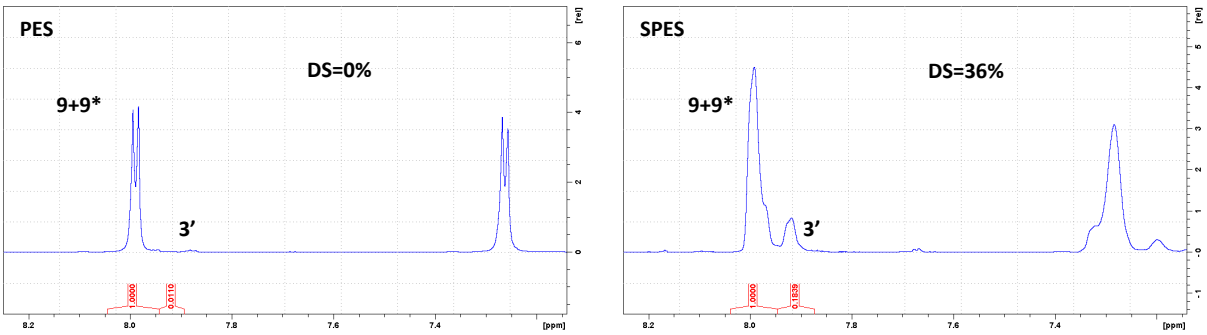

Figure 5. ^{1}H-NMR spectra of pure PES and SPES used in the development of composite membranes.

DS values obtained from the titration method (35.5%) and by ^{1}H-NMR (36%) matched extremely well and were consistent with the ion exchange capacity (IEC) per unit weight of dry polymer (1.36 ± 0.04

mmol/g). The obtained IEC is inside the range of IEC values observed for commercially available cation exchange membranes (0.8 to 3.5 mmol/g [32]).

3.2.2. Water uptake and surface hydrophilicity

In sulfonated polymers, the water uptake increases with the sulfonation degree. For pure PES there is a negligible water uptake, while for the composite-0% membrane, with DS 36%, it became significant (Figure 6).The molecular structure of SPES consists of a hydrophobic backbone and hydrophilic sulfonic acid groups. The hydrophilic part of the structure is mainly responsible for water uptake in polymers. Within the composite membranes, the increase of HMO content also leads to an increase in the water content since HMO has a hydrophilic nature [33,34].

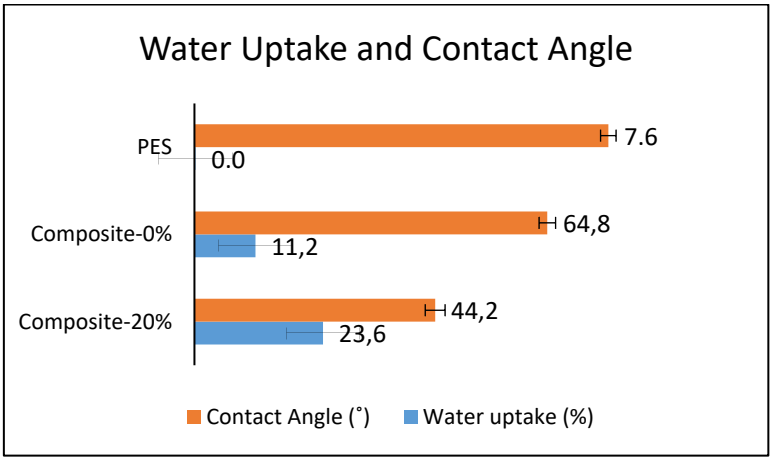

Figure 6. Comparison of water uptake and contact angle of pure polyethersulfone membrane and composite membranes.

The prepared membranes also showed the expected trend in contact angle. PES is mildly hydrophobic, with a contact angle value of 76 °, while an increase in DS leads to a slight decrease of the contact angle to around 65 ° for composite-0% membrane due to an increase in the hydrophilic part of its structure. For the composite-20% membrane, the contact angle further decreased due to the incorporation of the hydrophilic HMO filler.

3.2.3. FT-IR analysis

The FT-IR spectrum of LMO showed three main peaks at 1425 cm^{-1}, 860 cm^{-1} and 620 cm^{-1} (Figure 7). The absorption band at 1425 cm^{-1} indicates the symmetric stretching of C=O bonds in carbonate ions (from unreacted Li_2CO_3 and $MnCO_3$ during the fusion reaction to prepare LMO) while at 860 cm^{-1} the O-C-O bonds experiences bending. The peak at 620 cm^{-1} can be attributed to the stretching vibration of Mn-O [35,36]. Figure 7 also showed that after acid treatment (HMO spectrum), two peaks at 1425 cm^{-1} and 860 cm^{-1} vanished because of the reaction of hydrochloric acid with these unreacted carbonates.

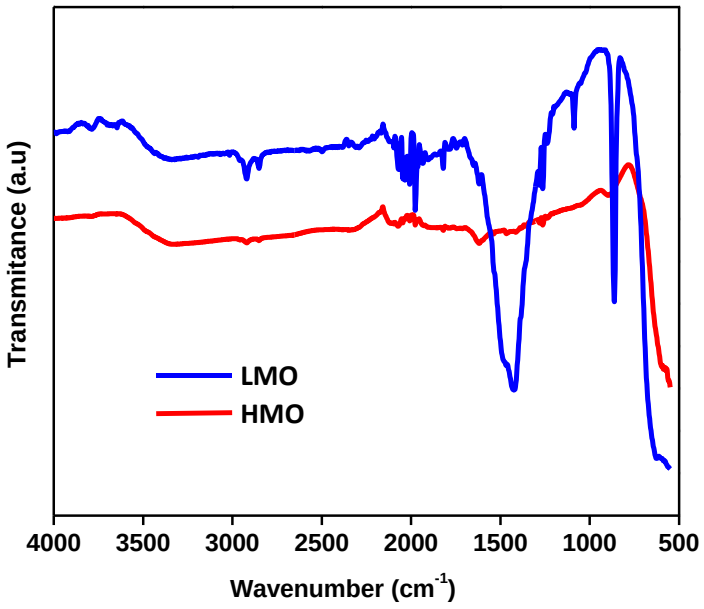

Figure 7. FT-IR spectra of lithium selective adsorbent.

For composite membranes, the typical peaks associated with the main backbone of the polymer were present in all spectra (Figure 8). A characteristic broad band at around 3480 cm^{-1} linked to the

vibrational stretching of hydroxyl (-OH) of the sulfonic acid groups whereas the other two peaks at 1307 and 1148 cm^{-1} (Figure 8) are the representative of the aromatic SO_3H groups which confirm the sulfonation [37]. The peak at 1031 cm^{-1} (characteristic for the S=O bond stretching) confirms the presence of lithium salt ($LiCF_3SO_3$) in the polymer matrix [38]. The absorbance at 640 cm^{-1} was due to Mn-O bond stretching which proves the presence of lithium adsorbent in the composite membranes [39].

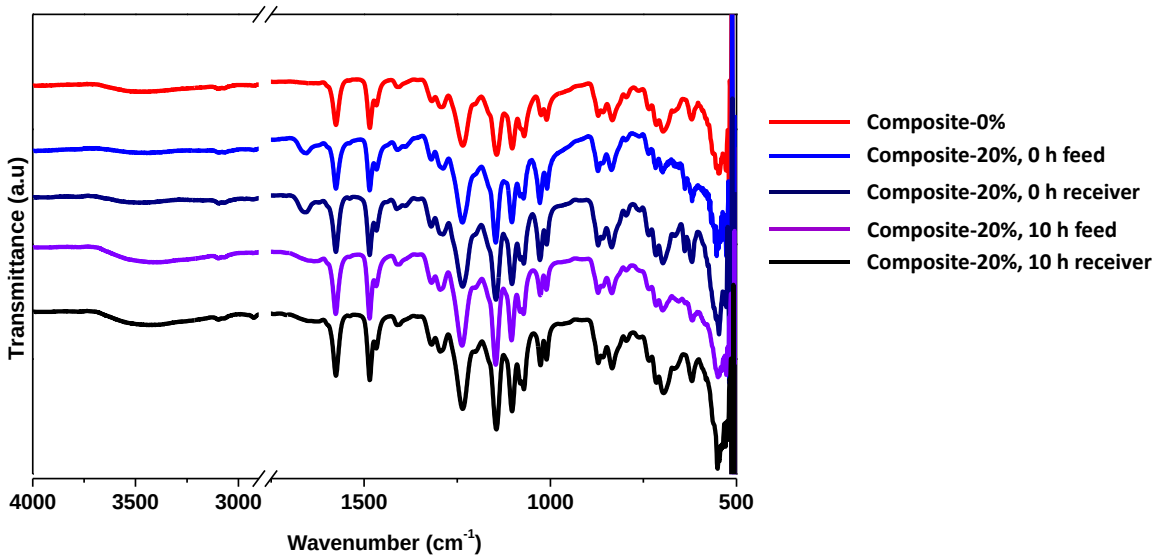

Figure 8. FT-IR spectra of the composite membranes.

All the characteristic peaks of the membrane remained unaffected after the use of the membrane during 10 hours in diffusion dialysis experiments, therefore the FT-IR analysis confirms that the chemical structure of the composite membrane is stable under the tested conditions.

3.2.4. XRD analysis

XRD was used to determine the morphology and crystallinity of the membranes and to measure the inter-planer distance (d). This tool could also be used to measure the average distance between the polymer chains. Figure 9a, 9b shows the diffractograms of the lithium selective adsorbent and composite-20% membrane respectively.

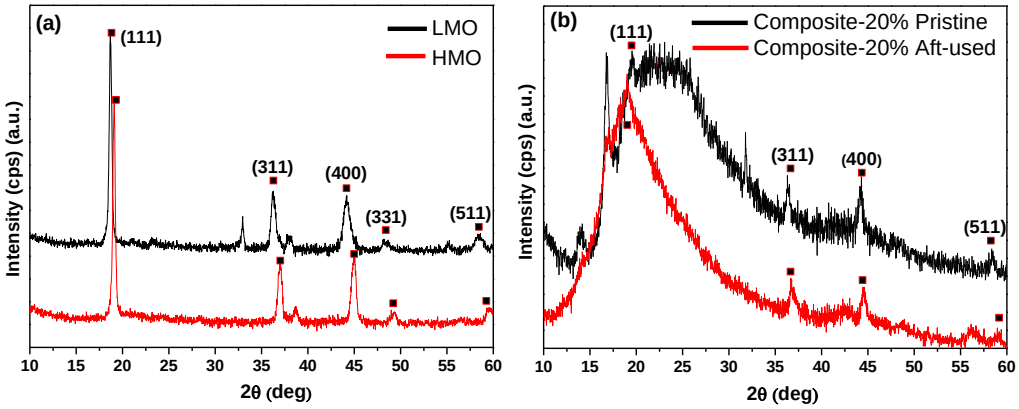

Figure 9. XRD spectra of (a) LMO and HMO, (b) composite-20% membrane pristine and after used.

The polymer chain packing of the composite-20% membrane before and after use was studied and compared with LMO and HMO. In both spectra of LMO and HMO there are five main common peaks at 2θ = 18.5 °, 36.5 °, 44.4 °, 48.5 ° and 58 ° which are correspond to the crystalline planes (111), (311), (400), (331) and (511) of spinel structure [40]. Other peak that only appeared at 2θ = 33.4 ° in LMO spectrum is due to the $MnCO_3$ impurity or leftover reactant in the synthesis of lithium adsorbent [41–43]. This peak disappeared in HMO spectrum due the reaction of $MnCO_3$ with HCl during acid leaching of lithium. Overall, XRD results testify that lithium adsorbent had spinel structure.

For the pristine composite-20% membrane, a typical amorphous halo appeared at 2θ = 22.7 ° (Figure 9b) that corresponds to an intermolecular average distance of 3.8 Å whereas, after being used, the

maximum of the amorphous halo centred at 2θ = 19.2 °, corresponding to an inter-planar distance of 4.5 Å, which depicts a looser polymer chains packing within the membrane structure, probably due to swelling which is directly related to the polymer hydrophilicity. By increasing the degree of sulfonation, the interaction of water molecules with the sulfonated parts of the polymer favours its swelling [44]. Moreover, some crystalline peaks with a low intensity were also detected with the same 2θ values as observed for the HMO powder.

The appearance of these peaks demonstrates that HMO maintained its crystalline structure inside the composite membrane, which is very important to grant the selective lithium transport through the membrane [45].

3.2.5. Morphology

The analysis of SEM images (Figure 10a-f) revealed that the pristine composite-0% membrane (Figure 10a) had a dense surface without visible defects. The incorporation of the HMO adsorbent promoted a certain roughness of the surface for the composite-20% membrane (Figure 10b). No drastic visible changes in the surface morphology of the composite-20% membrane were observed after being used (Figure 10c).

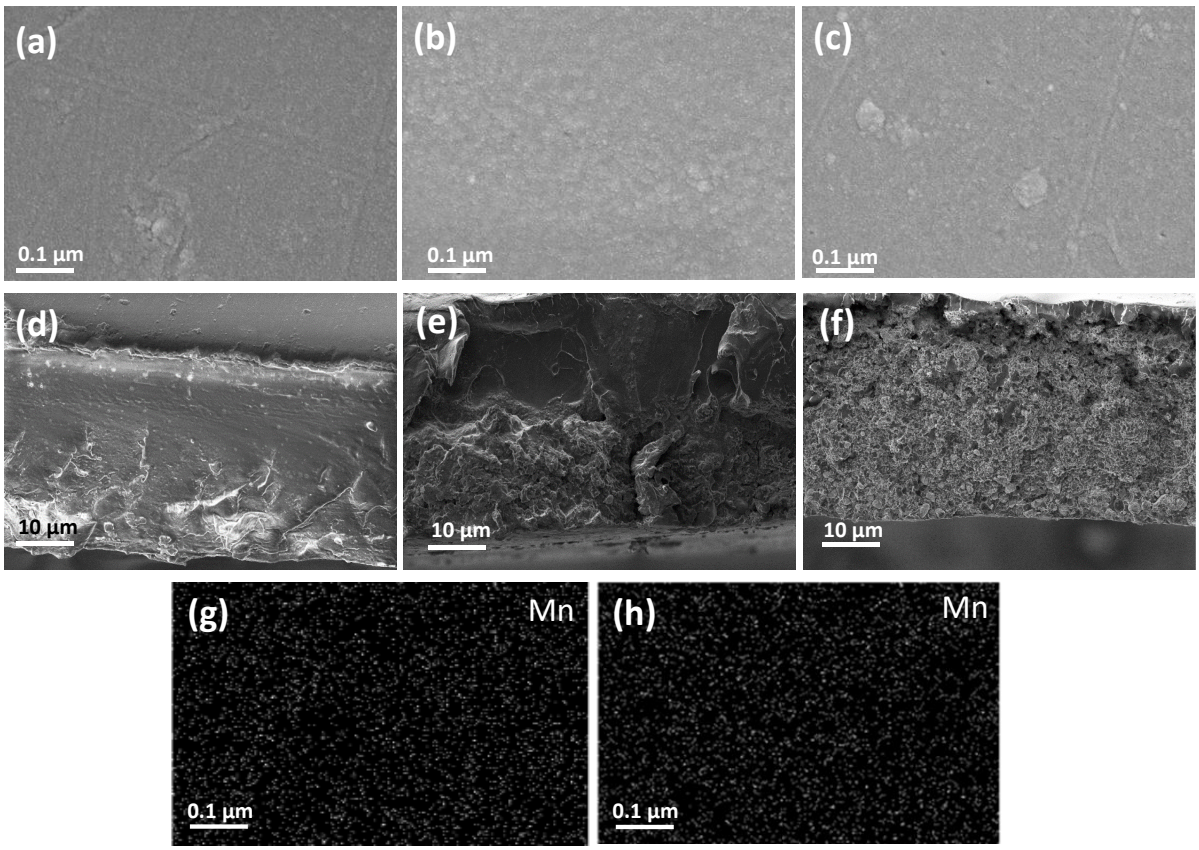

Figure 10. SEM images of (a) composite-0% surface, (b) composite-20% surface before use, (c) composite-20% surface after use, (d) composite-0% cross section, (e) composite-20% cross section before use, (f) composite-20% cross section after use, (g) EDX map for Mn atom on (b), (h) EDX map for Mn atom on (c).

The cross-section images (Figure 10d-f) show that the composite membrane exhibited a good compatibility between inorganic adsorbent and polymeric matrix, leading to a homogeneous and a uniform dispersion that was maintained after the membrane usage in diffusion experiments. The homogeneous distribution of the manganese (Mn) atom was confirmed by EDX maps for composite-20% membrane (Figure 10g, 10h). Moreover, a very small difference between the atomic composition of the pristine and used composite-20% membrane (22.95 ± 4.86% vs. 21.00 ± 3.25% for Mn, respectively) confirmed the stability of the inorganic component in the polymeric matrix, as expected based on FT-IR results (Figure 8 and Section 3.2.3.).

3.2.6. Thermal properties

Thermal properties of HMO, composite-0% and composite-20% membranes, calculated from TGA and DSC software, are compared and resumed in Figure 11 and Table 1 respectively. The TGA curve for the HMO adsorbent exhibited two weight loss steps. The first weight loss step (between 30 and 200 °C) is attributed to the water loss by the condensation of lattice hydroxyl groups and the second weight loss step (between 400 and 500 °C) is due to the degradation of functional groups at the surface of the adsorbent [16].

TGA curves (Figure11) and the corresponding thermal degradation values (Table 1) of the membranes confirm that the developed membranes are thermally stable. The membrane with 0% HMO content was thermally more stable (T_d onset= 330 °C) compared to the composite-20% membrane which degraded at lower temperature (T_d onset= 194 °C), most probably as a consequence of the addition of the HMO adsorbent which has relatively low thermal stability (T_d onset= 200 °C). The residue measured at 600 °C is the highest for HMO, as expected due to its inorganic nature and, consequently, the residue of composite-20% membrane is almost 15% higher comparing to the residue of the composite-0% membrane, due to the presence of HMO in the polymer matrix.

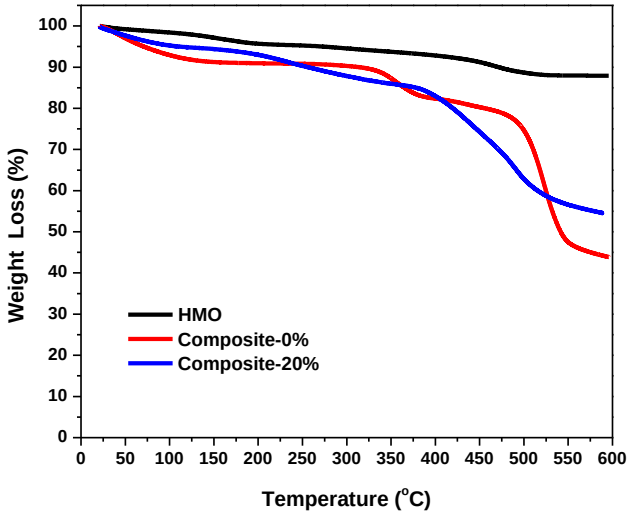

Figure 11. TGA curves of HMO and composite membranes.

Table 1. Thermal degradation, glass transition temperatures and residue values of different membrane samples and HMO.

Samples	T_d onset (°C)		Residue at 600°C (%)	T_g (°C)
	2nd step	3rd step		
HMO	200	400	92	-
Composite-0%	330	506	39	251
Composite-20%	194	403	55	197

The DSC curves of composite 0% and 20% membranes in Figure 12 showed a change in the heat capacity associated with the glass transition temperature (T_g), which means that the matrix has an amorphous structure in accordance with the XRD diffraction pattern (Figure 9b). T_g is an important property when considering amorphous polymers for a particular end-use and is defined as the temperature below which the physical properties of plastics change to those of a glassy or crystalline state [46]. Thus, the T_g reveals the mobility of the bulk matrix and any factor that favours this mobility will decrease the T_g. On the contrary, any factor that reduces the mobility will increase it. Therefore, the T_g mainly depends on the nature of the chemical and structural properties of the bulk material and polymers.

The T_g value of pure PES is 230 °C [47], and for the composite-0% membrane, it increased to 251 °C (Table 1). This can be attributed to the introduction of sulfonic acid groups into the polymer chain, which causes an increase of the intermolecular interactions between the polymer chains, resulting in a higher glass transition temperature. With the addition of HMO the T_g value decreased to 197 °C for the composite-20% membrane because the presence of an inorganic filler may constrain the intermolecular interaction between the polymer chains [21,48,49]. Finally, only one T_g is visible on the DSC curve of the composite-20% membrane, which is typical for composite systems with a good compatibility in terms of intermolecular interaction between inorganic and organic phases.

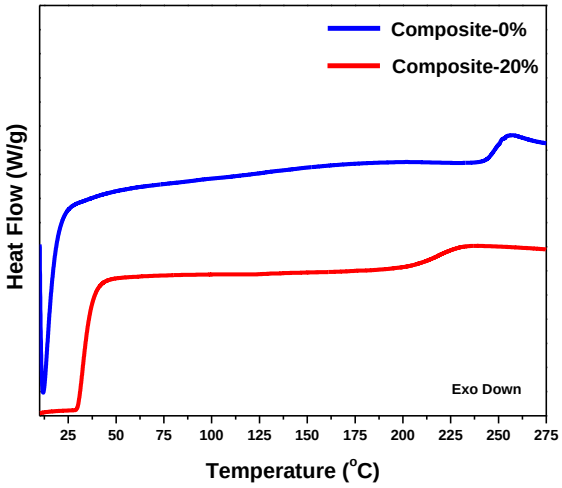

Figure 12. DSC curves of composite membrane.

3.2.7. Mechanical properties

Micro-hardness is a quick and easy technique for determining different mechanical properties by comparing the hardness values, which is the measure of material's ability to resist against stretching or indentation (plastic deformation) [28]. Micro-hardness and tensile strength of the membrane samples are summarized in Table 2.

Table 2. Mechanical properties of membranes

Membranes	Vickers Hardness (MPa)	Tensile Strength (MPa)
Composite-0%	107.9	46.3
Composite-20%	88.3	37.9

The tensile strength of composite-0% membrane was 46.29 MPa, which is higher than the tensile strength of the composite-20% membrane (37.9 MPa), nevertheless still enough to produce mechanically stable membranes. The lower mechanical strength of the composite-20% membrane is due to the interaction between the polymer and inorganic filler, as also indicated by the glass transition temperature (Section 3.2.6). These membranes are mechanically stronger (tensile strength = 37.9 MPa) compared to the HMO base polymeric lithium selective membranes reported in the literature (tensile strength = 24.7 MPa) [16].

4. CONCLUSION

- Composite lithium transport selective polymeric membranes were developed by merging hydrogen manganese oxide (HMO) into mixture of sulfonated polyethersulfone (SPES), sodium salt of polystyrene sulfonate (PSS-Na) and lithium triflate ($LiCF_3SO_3$).
- The uniform dispersion of the adsorbent within the sulfonated polymeric membranes was confirmed.
- The presence of HMO in the membrane not only improved its lithium selectivity, but also increased its hydrophilicity, which led to the increased ionic fluxes compared to those obtained with the membrane without HMO (composite-0%).
- The highest Li^+/Mg^{2+} ideal selectivity of 11.75 was achieved by the composite membrane containing 20% (w/w) of HMO.
- In diffusion dialysis, a Li^+/Mg^{2+} binary separation factor of 9.1 was achieved at a Li^+ flux of 0.026 mol/(m^2.h). In electro-diffusion dialysis, when a potential difference of + 0.2 V was applied, the transport performance was improved in terms of lithium flux (0.11 mol/(m^2.h)), while still maintaining a relatively high Li^+/Mg^{2+} binary separation factor of 5.0.
- The performed analyses proved that the prepared membranes are chemically and mechanically stable and adequate for use at large scale.

The use of lithium selective adsorbents with high adsorption capacity and polymers possessing high IEC could further improve the membrane performance. Overall, this study provides a strong base for the development of highly lithium selective membranes.

ACKNOWLEDGMENTS

This project has received funding from the European Union's Horizon 2020 research and innovation programme under grant agreement No 869467 (SEArcularMINE). This work was supported by the Associate Laboratory for Green Chemistry- LAQV, which is financed by Portuguese national funds from FCT/MCTES (UID/QUI/50006/2019). This work was also supported by "*Programa Operacional Regional de Lisboa, na componente FEDER*" and "*Fundação para a Ciência e Tecnologia*, I.P." through research project PTDC/EQU-EPQ/29579/2017. S. Pawlowski acknowledges *Fundação para a Ciência e Tecnologia*, I.P. for his Contract CEECIND/01617/2017. iNOVA4Health – UIDB/Multi/04462/2020, a program financially supported by Fundação para a Ciência e Tecnologia / Ministério da Educação e Ciência, through national funds is acknowledged. Funding from INTERFACE Programme, through the Innovation, Technology and Circular Economy Fund (FITEC), is also gratefully acknowledged. The authors also acknowledge Professor Rui Silva, from i3N/CENIMAT, Department of Materials Science, Faculty of Science and Technology (FCT), Universidade NOVA de Lisboa, for the support to analyse mechanical properties.

REFERENCES

[1] T. Ryu, Y. Haldorai, A. Rengaraj, J. Shin, H.J. Hong, G.W. Lee, Y.K. Han, Y.S. Huh, K.S. Chung, Recovery of Lithium Ions from Seawater Using a Continuous Flow Adsorption Column Packed with Granulated Chitosan-Lithium Manganese Oxide, Ind. Eng. Chem. Res. 55 (2016) 7218–7225. doi:10.1021/acs.iecr.6b01632.

[2] X. Xu, Y. Chen, P. Wan, K. Gasem, K. Wang, T. He, H. Adidharma, M. Fan, Extraction of lithium

with functionalized lithium ion-sieves, Prog. Mater. Sci. 84 (2016) 276–313. doi:10.1016/j.pmatsci.2016.09.004.

[3] B. Swain, Recovery and recycling of lithium: A review, Sep. Purif. Technol. 172 (2017) 388–403. doi:10.1016/j.seppur.2016.08.031.

[4] D. Gu, W. Sun, G. Han, Q. Cui, H. Wang, Lithium ion sieve synthesized via an improved solid state method and adsorption performance for West Taijinar Salt Lake brine, Chem. Eng. J. 350 (2018) 474–483. doi:10.1016/j.cej.2018.05.191.

[5] P.K. Choubey, K.S. Chung, M. seuk Kim, J. chun Lee, R.R. Srivastava, Advance review on the exploitation of the prominent energy-storage element Lithium. Part II: From sea water and spent lithium ion batteries (LIBs), Miner. Eng. 110 (2017) 104–121. doi:10.1016/j.mineng.2017.04.008.

[6] M.J. Park, G.M. Nisola, E.L. Vivas, L.A. Limjuco, C.P. Lawagon, J.G. Seo, H. Kim, H.K. Shon, W.J. Chung, Mixed matrix nanofiber as a flow-through membrane adsorber for continuous Li+ recovery from seawater, J. Memb. Sci. 510 (2016) 141–154. doi:10.1016/j.memsci.2016.02.062.

[7] Y. Zhang, L. Wang, W. Sun, Y. Hu, H. Tang, Membrane technologies for Li+/Mg2+ separation from salt-lake brines and seawater: A comprehensive review, J. Ind. Eng. Chem. 81 (2020) 7–23. doi:10.1016/j.jiec.2019.09.002.

[8] A. Razmjou, M. Asadnia, E. Hosseini, A. Habibnejad Korayem, V. Chen, Design principles of ion selective nanostructured membranes for the extraction of lithium ions, Nat. Commun. 10 (2019). doi:10.1038/s41467-019-13648-7.

[9] H. Vikström, S. Davidsson, M. Höök, Lithium availability and future production outlooks, Appl. Energy. 110 (2013) 252–266. doi:10.1016/j.apenergy.2013.04.005.

[10] X.Y. Nie, S.Y. Sun, Z. Sun, X. Song, J.G. Yu, Ion-fractionation of lithium ions from magnesium

ions by electrodialysis using monovalent selective ion-exchange membranes, Desalination. 403 (2017) 128–135. doi:10.1016/j.desal.2016.05.010.

[11] L. Xing, J. Song, Z. Li, J. Liu, T. Huang, P. Dou, Y. Chen, X.M. Li, T. He, Solvent stable nanoporous poly (ethylene-co-vinyl alcohol) barrier membranes for liquid-liquid extraction of lithium from a salt lake brine, J. Memb. Sci. 520 (2016) 596–606. doi:10.1016/j.memsci.2016.08.027.

[12] H.J. Cassady, E.C. Cimino, M. Kumar, M.A. Hickner, Specific ion effects on the permselectivity of sulfonated poly(ether sulfone) cation exchange membranes, J. Memb. Sci. 508 (2016) 146–152. doi:10.1016/j.memsci.2016.02.048.

[13] Y. Guo, Y. Ying, Y. Mao, X. Peng, B. Chen, Polystyrene Sulfonate Threaded through a Metal–Organic Framework Membrane for Fast and Selective Lithium-Ion Separation, Angew. Chemie - Int. Ed. 55 (2016) 15120–15124. doi:10.1002/anie.201607329.

[14] T. Hoshino, Innovative lithium recovery technique from seawater by using world-first dialysis with a lithium ionic superconductor, Desalination. 359 (2015) 59–63. doi:10.1016/j.desal.2014.12.018.

[15] J. Wang, Y. Liu, H. Zhang, Y. Li, H. Bai, W. Wu, Z. Li, X. Zhang, Embedding sulfonated lithium ion-sieves into polyelectrolyte membrane to construct efficient proton conduction pathways, J. Memb. Sci. 501 (2016) 109–122. doi:10.1016/j.memsci.2015.12.008.

[16] J. Zhang, X. Cui, F. Yang, L. Qu, F. Du, H. Zhang, J. Wang, Hybrid Cation Exchange Membranes with Lithium Ion-Sieves for Highly Enhanced Li+ Permeation and Permselectivity, Macromol. Mater. Eng. 304 (2019) 1–11. doi:10.1002/mame.201800567.

[17] H.J. Hong, I.S. Park, T. Ryu, J. Ryu, B.G. Kim, K.S. Chung, Granulation of Li1.33Mn1.67O4 (LMO) through the use of cross-linked chitosan for the effective recovery of Li+ from seawater, Chem. Eng. J. 234 (2013) 16–22. doi:10.1016/j.cej.2013.08.060.

[18] T. Ryu, D.H. Lee, J.C. Ryu, J. Shin, K.S. Chung, Y.H. Kim, A lithium selective adsorption composite by coating adsorbent on PVC plate using epoxy-silica hybrid binder, Hydrometallurgy. 183 (2019) 118–124. doi:10.1016/j.hydromet.2018.11.011.

[19] K.S. Chung, J.C. Lee, W.K. Kim, S.B. Kim, K.Y. Cho, Inorganic adsorbent containing polymeric membrane reservoir for the recovery of lithium from seawater, J. Memb. Sci. 325 (2008) 503–508. doi:10.1016/j.memsci.2008.09.041.

[20] K. Noel Jacob, S. Senthil Kumar, A. Thanigaivelan, M. Tarun, D. Mohan, Sulfonated polyethersulfone-based membranes for metal ion removal via a hybrid process, J. Mater. Sci. 49 (2014) 114–122. doi:10.1007/s10853-013-7682-1.

[21] A. Noshay, L.M. Robeson, Sulfonated polysulfone, J. Appl. Polym. Sci. 20 (1976) 1885–1903. doi:10.1002/app.1976.070200717.

[22] D. Lu, H. Zou, R. Guan, H. Dai, L. Lu, Sulfonation of polyethersulfone by chlorosulfonic acid, Polym. Bull. 54 (2005) 21–28. doi:10.1007/s00289-005-0361-x.

[23] R. Guan, H. Zou, D. Lu, C. Gong, Y. Liu, Polyethersulfone sulfonated by chlorosulfonic acid and its membrane characteristics, Eur. Polym. J. 41 (2005) 1554–1560. doi:10.1016/j.eurpolymj.2005.01.018.

[24] R. Guan, H. Dai, C. Li, J. Liu, J. Xu, Effect of casting solvent on the morphology and performance of sulfonated polyethersulfone membranes, J. Memb. Sci. 277 (2006) 148–156. doi:10.1016/j.memsci.2005.10.025.

[25] B. Van Der Bruggen, Chemical modification of polyethersulfone nanofiltration membranes: A review, J. Appl. Polym. Sci. 114 (2009) 630–642. doi:10.1002/app.30578.

[26] H. Komber, S. Chakraborty, B. Voit, S. Banerjee, Degree of sulfonation and microstructure of post-sulfonated polyethersulfone studied by NMR spectroscopy, Polymer (Guildf). 53 (2012) 1624–1631. doi:10.1016/j.polymer.2012.02.020.

[27] W.H. Bragg, The reflection of X-rays by crystals [3], Nature. 91 (1913) 477. doi:10.1038/091477b0.

[28] A. Linares, R. Benavente, Effect of sulfonation on thermal, mechanical, and electrical properties of blends based on polysulfones, Polym. J. 41 (2009) 407–415. doi:10.1295/polymj.PJ2008252.

[29] P. Zhang, S.X. Li, Z.F. Zhang, General relationship between strength and hardness, Mater. Sci. Eng. A. 529 (2011) 62–73. doi:10.1016/j.msea.2011.08.061.

[30] T. Koch, S. Seidler, Correlations between indentation hardness and yield stress in thermoplastic polymers, Strain. 45 (2009) 26–33. doi:10.1111/j.1475-1305.2008.00468.x.

[31] W.K. Setiawan, K.Y. Chiang, Silica applied as mixed matrix membrane inorganic filler for gas separation: A review, Sustain. Environ. Res. 1 (2019). doi:10.1186/s42834-019-0028-1.

[32] E.M.V. Hoek, V. V. Tarabara, Y. Wang, T. Xu, Ion Exchange Membranes, in: Encycl. Membr. Sci. Technol., John Wiley & Sons, Inc., Hoboken, NJ, USA, 2013: pp. 1–58. doi:10.1002/9781118522318.emst005.

[33] F. Wang, M. Hickner, Y.S. Kim, T.A. Zawodzinski, J.E. McGrath, Direct polymerization of sulfonated poly(arylene ether sulfone) random (statistical) copolymers: Candidates for new proton exchange membranes, J. Memb. Sci. 197 (2002) 231–242. doi:10.1016/S0376-7388(01)00620-2.

[34] T.D. Gierke, G.E. Munn, F.C. Wilson, Morphology in Nafion Perfluorinated Membrane Products, As Determined By Wide- and Small-Angle X-Ray Studies., J. Polym. Sci. Part A-2, Polym. Phys. 19 (1981) 1687–1704. doi:10.1002/pol.1981.180191103.

[35] E. Alibakhshi, E. Ghasemi, M. Mahdavian, B. Ramezanzadeh, Corrosion inhibitor release from Zn-Al-[PO43-]-[CO32-] layered double hydroxide nanoparticles, Prog. Color. Color. Coatings. 9 (2016) 233–248.

[36] F.A. Miller, C.H. Wilkins, Infrared Spectra and Characteristic Frequencies of Inorganic Ions, Anal. Chem. 24 (1952) 1253–1294. doi:10.1021/ac60068a007.

[37] M.R. Pereira, J. Yarwood, ATR-FTIR spectroscopic studies of the structure and permeability of sulfonated poly(ether sulfone) membranes: Part 1. - Interfacial water-polymer interactions, J. Chem. Soc. - Faraday Trans. 92 (1996) 2731–2735. doi:10.1039/FT9969202731.

[38] P. Tamilselvi, M. Hema, Effect of plasticizer on poly (vinyl alcohol): Poly (vinylidene fluoride) blend polymer electrolyte, Int. J. ChemTech Res. 6 (2014) 5265–5269.

[39] M. Zheng, H. Zhang, X. Gong, R. Xu, Y. Xiao, H. Dong, X. Liu, Y. Liu, A simple additive-free approach for the synthesis of uniform manganese monoxide nanorods with large specific surface area, Nanoscale Res. Lett. 8 (2013) 1–7. doi:10.1186/1556-276X-8-166.

[40] F. Xue, B. Wang, M. Chen, C. Yi, S. Ju, W. Xing, Fe3O4-doped lithium ion-sieves for lithium adsorption and magnetic separation, Sep. Purif. Technol. 228 (2019). doi:10.1016/j.seppur.2019.115750.

[41] Q.X. Xia, K. San Hui, K.N. Hui, S.D. Kim, J.H. Lim, S.Y. Choi, L.J. Zhang, R.S. Mane, J.M. Yun, K.H. Kim, Facile synthesis of manganese carbonate quantum dots/Ni(HCO3)2-MnCO3 composites as advanced cathode materials for high energy density asymmetric supercapacitors, J. Mater. Chem. A. 3 (2015) 22102–22117. doi:10.1039/c5ta04005a.

[42] Y. Han, H. Kim, J. Park, Millimeter-sized spherical ion-sieve foams with hierarchical pore structure for recovery of lithium from seawater, Chem. Eng. J. 210 (2012) 482–489. doi:10.1016/j.cej.2012.09.019.

[43] M.Y. Nassar, A.S. Amin, I.S. Ahmed, S. Abdallah, Sphere-like Mn2O3 nanoparticles: Facile hydrothermal synthesis and adsorption properties, J. Taiwan Inst. Chem. Eng. 64 (2016) 79–88. doi:10.1016/j.jtice.2016.03.041.

[44] W.Y. Chuang, T.H. Young, D.M. Wang, R.L. Luo, Y.M. Sun, Swelling behavior of hydrophobic

polymers in water/ethanol mixtures, Polymer (Guildf). 41 (2000) 8339–8347. doi:10.1016/S0032-3861(00)00176-2.

[45] R.M. Huertas, C.M. Doherty, A.J. Hill, A.E. Lozano, J. de Abajo, J.G. de la Campa, E.M. Maya, Preparation and gas separation properties of partially pyrolyzed membranes (PPMs) derived from copolyimides containing polyethylene oxide side chains, J. Memb. Sci. 409–410 (2012) 200–211. doi:10.1016/j.memsci.2012.03.057.

[46] Z.-J. Zhao, S.H. Hwang, H.-J. Kang, S. Jeon, M. Bok, S. Ahn, D. Im, J. Hahn, H. Kim, J.-H. Jeong, Adhesive-Layer-Free and Double-Faced Nanotransfer Lithography for a Flexible Large-Area MetaSurface Hologram, ACS Appl. Mater. Interfaces. 12 (2020) 1737–1745. doi:10.1021/acsami.9b14345.

[47] J. Chen, Q. Guo, Z. Zhao, X. Wang, C. Duan, Structures and mechanical properties of PEEK/PEI/PES plastics alloys blent by extrusion molding used for cable insulating jacketing, Procedia Eng. 36 (2012) 96–104. doi:10.1016/j.proeng.2012.03.016.

[48] M. Pirali-Hamedani, S. Mehdipour-Ataei, Effect of sulfonation degree on molecular weight, thermal stability, and proton conductivity of poly(arylene ether sulfone)s membrane, Des. Monomers Polym. 20 (2017) 54–65. doi:10.1080/15685551.2016.1231035.

[49] Y. Gao, G.P. Robertson, M.D. Guiver, X. Jian, Synthesis and characterization of sulfonated poly(phthalazinone ether ketone) for proton exchange membrane materials, J. Polym. Sci. Part A Polym. Chem. 41 (2003) 497–507. doi:10.1002/pola.10601.

ABBREVIATIONS

CEM	Cation exchange membrane
CAS	Chlorosulfonic acid
DS	Degree of sulfonation

DCS	Differential scanning calorimetry
DMF	Dimethylformamide
FTIR	Fourier transform infrared spectroscopy
HMO	$H_{1.33}Mn_{1.67}O_4$ (Hydrogen manganese oxide)
H-NMR	Nuclear magnetic resonance of proton
ICP-AES	Inductively coupled-plasma atomic emission spectroscopy
IEC	Ion exchange capacity
LMO	$Li_{1.33}Mn_{1.67}O_4$ (Lithium manganese oxide)
LIS	Lithium ion sieve
LSV	Linear sweep voltammetry
MOF	Metal organic framework
MH	Micro hardness
PES	Polyethersulfone
PSS-Na	Sodium salt of polystyrene sulfonate
SEM	Scanning electron microscopy
SPES	Sulfonated polyethersulfone
TGA	Thermogravimetric analysis
XRD	X-Ray diffraction
WC	Water content